This article has been accepted for publication in a future issue of this journal, but has not been fully edited. Content may change prior to final publication. Citation information: DOI 10.1109/TEC.2018.2815564, IEEE Transactions on Energy Conversion

Design and Control of a Decoupled Rotary-Linear Switched Reluctance Motor

Siyang Li, K.W.E Cheng, *Senior Member, IEEE*, Norbert Cheung, *Senior Member, IEEE*, and Yu Zou

***Abstract*—A decoupled two-degree of freedom (2-DOF) in the linear and rotary directions of a motor based on switched reluctance principle is investigated. First, the structure of the motor is introduced, and the design procedure for the main parameters of the motor is elaborated. Also, the magnetic decoupled structure for the motor is illustrated. Secondly, a magnetic circuit analysis is given to explain the decoupled structure, followed by simulation finite element method (FEM), including the inductance profiles, force and torque outputs etc. Meanwhile, control method for this motor is provided by using two proportional-integral-derivation (PID) controllers to regulator the linear position and the rotating angle independently. Linear force distribution function (FDF) and torque sharing function (TSF) are employed by the control system. Thirdly, experimental results involving the force and torque measurements, linear position and rotating angle responses are obtained, under specific loads and without a load. The motor is capable of realizing high-precision rotary and linear tracking within 0.3° and 500 μm under specific loading conditions, respectively. It suggests that the proposed structure can readily realize decoupled control proposed by this paper.**

***Index Terms*—2-DOF, Switched Reluctance Motor, PID, FEM.**

NOMENCLATURE

p	Pole width (mm)
q	Slot width (mm).
τ	Pole pitch (mm).
n	Mover yoke length (mm).
h	Stator width (mm).
g	Air gap length (mm).
d	Phase separation distance (mm).
s	Stator height (mm).
w	Stator width per stator element (mm).
l	Stack length (mm).
y	Mover leg width (mm).
a	Acceleration (m/s2).
v	Velocity (m/s).
M	Mass of the moving platform (kg).
f	Force (N).
P_w	Power (W).
P	Permeance (Wb/A).
L	Inductance (H).
λ	Inductance ratio.
A	Electric loading (A/m).
B	Flux density (T).
B_δ	Magnetic load (T).
z	Number of stator poles per stator element.
m	Number of stator element.
R	Reluctance (A/Wb).
F	Magnetomotive force (A).
ψ	Flux linkage (Wb・t).
Φ	Flux (Wb).
x	Position (mm).
R_{sy}	Reluctance of the stator yoke
R_{st}	Reluctance of the stator teeth
R_{sg}	Air gap reluctance between the outside stator and the mover.
R_{my}	Reluctance of the mover yoke
R_{mt}	Reluctance of the mover teeth
R_{mg}	Air gap reluctance between the mover and the inner stator.
R_{st1}	Reluctance of the inner stator teeth
R_{sy1}	Reluctance of the inner stator yoke
F_1	Magnetic motive force of the outside stator coil
F_2	Magnetic motive force of the inner stator coil

I. INTRODUCTION

Rotary-linear switched reluctance motors (RLSRMs) are usually implemented in industry applications, such as boring mill, drill press and carving machines, etc [1], [2]. Conventional machines are described in [3], [4], and such motions are commonly realized by two independent motors with mechanical connecting parts. However, the traditional designs cannot avoid the drawbacks of complex mechanical structures and control methods, thus reducing their tracking accuracy. The proposed direct-drive machine has the advantages of a high tracking accuracy and simplified mechanical configuration that be applied extensively in industry.

In [5]-[7], the principles of actuator based on the permanent magnet (PM) synchronous motor are discussed. However, it is not suitable for movements of rotary and linear, because of its complex control method and operating environment restriction. Also, PMs are vulnerable to high temperature and vibrations that can lead to permanent demagnetization. There are other

This article has been accepted for publication in a future issue of this journal, but has not been fully edited. Content may change prior to final publication. Citation information: DOI 10.1109/TEC.2018.2815564, IEEE Transactions on Energy Conversion

configurations focused on induction motors [8], and stepper motors [9]. Unfortunately, they are all not widely employed by industry, due to their complexity or inefficiency. Moreover, the switched reluctance (SR) machines are suited for many industries, because of the advantages of the mechanical stability and structure simplicity [10]. An RLSRM has been presented to integrate rotating and linear motion together [11], [12] but the nonlinear method for linear motion [13] is desirable and a coupling effect has occurred when both rotary and linear motion are produced by the same coils. Therefore, the decoupled control methods have been investigated in [14].

In this paper, a novel RLSRM is investigated. Its property of physical decoupled structure has been extensively investigated, while the tracking precision is increased with a simple control scheme, and the proposed structure is verified by finite element method (FEM). The experimental results prove that the structure is stable and effectiveness and the errors of rotary and position tracking can be controlled within 0.3˚and 500 μm for the rotary and linear axis, respectively.

II. Motor Structure

The RLSRM combines a 4-phase linear machine and a 3-phase rotary motor together as shown in Fig.1 (a). The basic specifications are listed in Table I. The outside part controls the moving shaft for linear motion, as well as the inside drives for rotary motion. Both parts have teeth and slots. The core of the machine is the stator core of the rotary section with a shaft. The mover that can realize rotary and linear movements is fixed on the shaft by using two bearings. This mover is fully embraced by a solid aluminum structure. The linear stator is connected and fixed on the outside stator base of the RLSRM. According to the structure, the mover is completely decoupled in magnetic circuits for the linear and rotary movements. Consequently, the manufacturing difficulty has been overcome. Moreover, the linear and rotary movements can be controlled individually, and there is no electromagnetic interference between them. With the optimizing and simplifying the control method, the high-precision tracking can be also realized. The main specifications of the motor are listed in Table I. Fig.1 (b) shows the structure of the mover. This mover has poles and slots deployed alternatively and their lengths are listed in Table I. The section view of the motor including the mover, the outside stator and the inner stator is shown in Fig.1 (c).

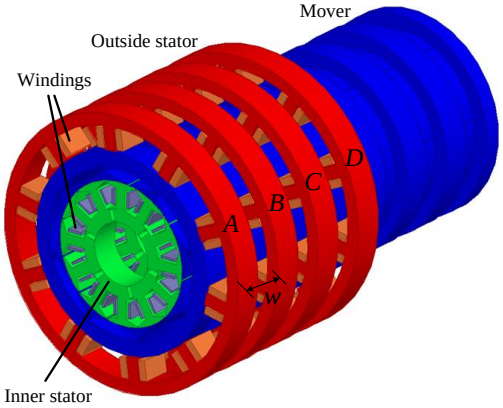

(a)

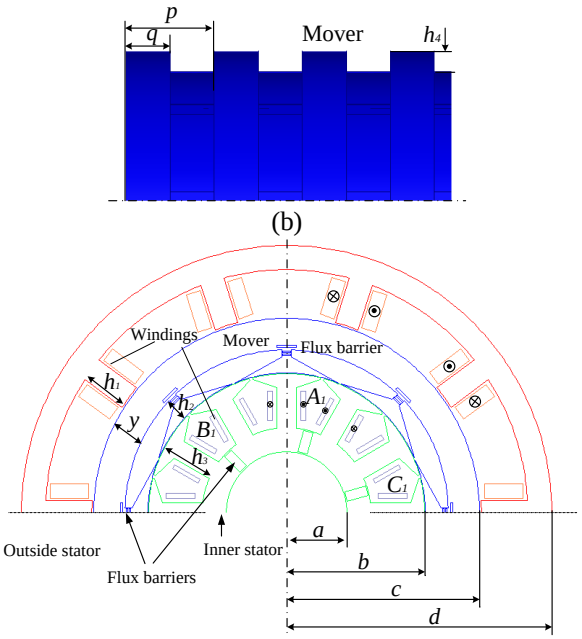

(b)

(c)

Fig.1The structure of the proposed motor (a) and section views the mover (b) and the motor (c).

TABLE I
THE MAIN SPECIFICATIONS OF THE MOTOR

Symbol	Value (unit)
P	500 W
U	80 V
I	6 A
y	10 mm
a	25 mm
b	60 mm
c	80 mm
d	110 mm
p	46 mm
q	24 mm
h1	19.2 mm
h2	9.5 mm
h3	22.4 mm
h4	10 mm
g1	0.8 mm
g2	0.3 mm
Length of outside stator	92 mm
Length of inner stator	200 mm
Length of the mover	400 mm
Encoder accuracy	1μm

This motor has a decoupled magnetic circuit structure between the two stators, which means that flux lines generated from the outside stator cannot pass through the mover to reach the inner stator. Both the two stators adopt short flux paths with the mover. Therefore, there is no magnetic influence between the two stators. Control methods to the motor could be very simple due to the decoupled structure. The movements in the two directions can be realized simultaneously and controlled independently, thus reaching a high precision linear position tracking and rotating control.

This article has been accepted for publication in a future issue of this journal, but has not been fully edited. Content may change prior to final publication. Citation information: DOI 10.1109/TEC.2018.2815564, IEEE Transactions on Energy Conversion

III. Theoretical Analysis

A. The Linear Section

The exacted specifications of the linear section include the maximum linear velocity of 1.0 m/s, and the acceleration time of 0.267 s. So the acceleration can be defined by:

$$a = 3.75 \ \mathrm{m/s^2} \tag{1}$$

The maximum mass for mover is 40 *kg*. Then, average thrust force can be calculated as:

$$F = M \cdot a = 149.5 \ \mathrm{N} \tag{2}$$

The power capacity is given by:

$$P = F \cdot v = 149.5 \ \mathrm{W} \tag{3}$$

The electric load A and magnetic load B of the motor are designed as 30714 A/m and 1.2 T respectively. Assuming that the full duty cycle for the motor during current conducting in the positions where the inductance profile goes up is given, with efficiency at 60%, the air gap length can be ensured at 0.7 mm for limitation of manufacturing. The pole pitch of the outside stator can then be obtained by using the following equation [15]

$$w = \frac{P}{K_e \cdot K_d \cdot K_1 \cdot K_2 \cdot l \cdot v \cdot B \cdot A \cdot m} \tag{4}$$

where K_e is efficiency of the motor. K_d is the duty cycle of current conducting region in rising inductance areas. K_1 and K_2 are coefficients determined by the structure of the motor and the its inductance profiles. m is the number of the phases.

According to Ampere's law, when the rated current is 6 A and H_l =4000 A and l_a =18 mm, the number of turns per coil can be calculated as [16]

$$N = \frac{H_g(2g) + H_l \cdot l_a}{I} = 120 \tag{5}$$

H_g and H_l are magnetic intensities in the air gaps and the soft magnetic material of steel.

B. The Rotary Section

q is the number of phases. e_a and i_a are the induced electromotive force and current in phase winding, respectively. K_d is load factor of each phase in a switching period. Then, the electromagnetic power is calculated as:

$$P_{em} = q \cdot e_a \cdot i_a \cdot K_d = 400 \ \mathrm{W} \tag{6}$$

D_a is the diameter of rotor, and N_r is the number of rotor poles. The rotor pole pitch is:

$$\tau_r = \pi \cdot \frac{D_a}{N_r} \tag{7}$$

ϕ is the main flux with each θ_{off}, and l_δ is the length of stator base. Therefore, the magnetic load is defined by:

$$B_\delta = \frac{\phi}{\tau_r \cdot l_\delta} \tag{8}$$

The electromagnetic torque is given by

$$T_{em} = \frac{P_{em}}{\omega} = 6.71 \ \mathrm{Nm} \tag{9}$$

According to the winding current I, and N_{ph} for the number of turns of each phase winding. The electrical load can be calculated as [17]

$$A = \frac{q \cdot N_{ph} \cdot I}{\pi \cdot D_{si}} \tag{10}$$

Based on the cross-sectional area of conductor S_a, the electric current density is calculated [18]

$$J = \frac{I}{S_a} = \frac{\pi \cdot D_a \cdot A}{q \cdot N_{ph} \cdot S_a} = 5.006 \ \mathrm{A/mm^2} \tag{11}$$

C. Magnetic Circuit Analysis

As illustrated in Fig. 2 (a), the equivalent magnetic path for quarter part of the motor can be approximated shown using flux reluctance paths, neglecting flux leakage.

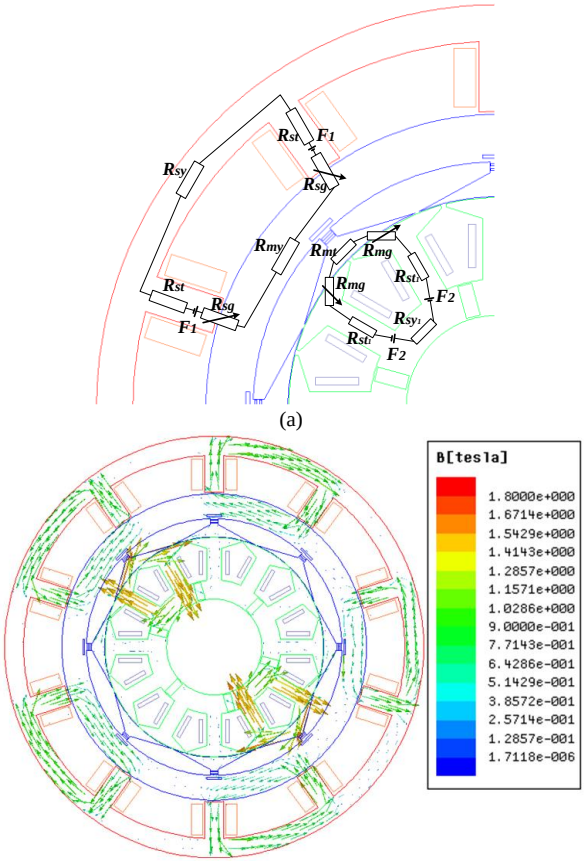

(a)

(b)

Fig.2 Equivalent magnetic path (a) and the flux density distribution of the motor (b)

From Fig.2 (a), there are two flux loops. The outside one closes from the mover and the outside stator. The inner loop flux lines are closed through the inner stator and the mover. According to Kirchhoff magnetic circuit rules, the two magnetic loops can be expressed as [19]

$$\phi_1 = \frac{2F_1}{R_{sy} + R_{my} + 2(R_{st} + R_{sg})} \tag{12}$$

$$\phi_2 = \frac{2F_2}{R_{sy1} + R_{mt} + 2(R_{st1} + R_{mg})} \tag{13}$$

ϕ_1 and ϕ_2 are flux along the first loop and the second loop. From the two equations, the two flux loops are separated magnetically. It means that the flux lines generated from the outside stator and the inner stator are decoupled and the motor

This article has been accepted for publication in a future issue of this journal, but has not been fully edited. Content may change prior to final publication. Citation information: DOI 10.1109/TEC.2018.2815564, IEEE Transactions on Energy Conversion

can be controlled individually in linear direction and rotary motion. The flux lines are shown in Fig.2 (b).

Generally, the magnetic flux generated by the outside stator is likely to pass through the triangle like shaped part and links the inner stator, producing a coupling effect. This effect would put an adverse effect on the performance of the motor because the outside stator could generate torque for the mover and the inner stator could also produce linear force output. For the motor proposed, there are two key techniques to avoid the coupling effect. Firstly, short flux paths for both the outside stator and the inner stator is designed. By doing so, the flux generated from the windings of the outside stator will close along two adjacent poles. Also, flux produced by each phase of the inner stator will also close along the triangle like shaped part, as shown in Fig.2 (b). These flux lines cannot be tangled with each other. Secondly, flux barriers in the mover are designed. The barriers can isolate the flux from the outside stator and that from the inner stator by increasing the magnetic reluctance between the outside part and the inner part of the mover. But the mover is still constructed by a steel plate only. Consequently, a decoupled magnetic structure for the motor is realized by using a simple way. From Fig.2 (b), the outside flux loops are totally separated with the inner flux loops, which fully illustrates the decoupled structure of the motor in the linear and rotary dimensions.

To further investigate the decoupled structure, the torque outputs of the motor under 6 A are estimated and shown in Fig.3, with the outside stator windings passing the currents from 0 A to 8 A. Although the torque fluctuates a little at 7 N.m, the linear motion has little influence on this torque. It shows that this 2D motor is physically decoupled and there is no magnetic influence between the outside and inner stators.

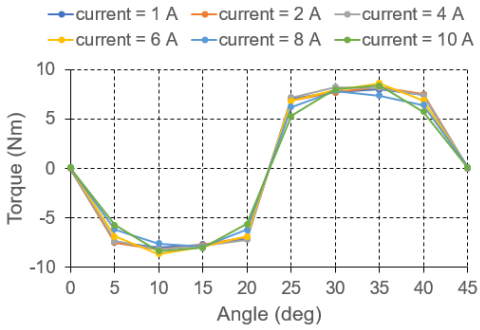

Fig. 3 Torque output profiles when outside stator is excited.

IV. Output Performance Prediction and Optimization

A. Output Performance

To fully investigate the motor performance, a 3-D finite element model is constructed. Fig.4 (a) shows the force output of the mover. The magnetic force reduces gradually from an unaligned position to an aligned position. When the excitation current is 10 A, the value of the force output reaches the peak up to 160 N at the position is around 4 mm. Likewise, the torque output profiles are given in Fig.4 (b) in a period. It can be seen that the value of torque increases to nearly 6.5 Nm when the mover rotates to 15 degrees from an aligned position to an unaligned position. Corresponding to the torque output profiles, inductance values of the windings embraced on a phase of the inner stator are also calculated, from aligned positions to unaligned positions as shown in Fig.4 (c). The maximum value of the inductance is 150 mH, nearly 3.7 times larger than that of the minimum inductance at unaligned positions.

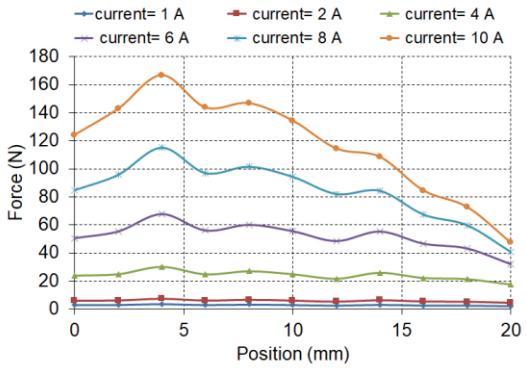

(a) Waveforms of FEM calculation of linear section.

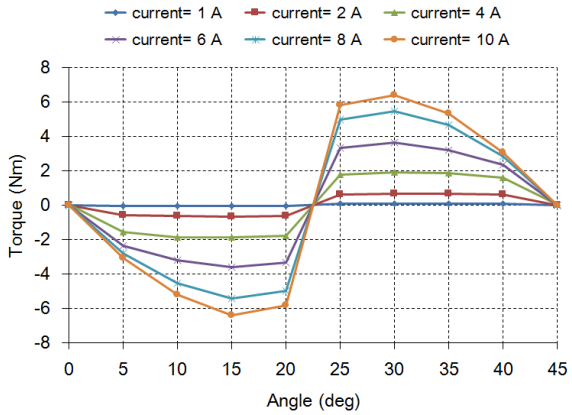

(b)waveforms of FEM calculation of rotary section.

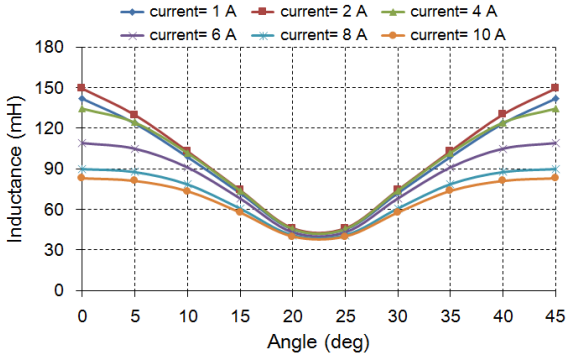

(c)Inductance performance of the linear part.

Fig.4 3D FEM calculations of the motor on force outputs (a), torque outputs (b) and inductance profiles (c).

B. Mover yoke optimization

In order to obtain the optimized yoke thickness of the mover, calculations via FEM on torque output of the motor are given in Fig. 5. When the excitation currents of the outside stator are imposed at 6 A and 10 A, torque outputs of the mover are compared. The torque deviations under the two excitation levels are small when the thickness of the yoke is 10 mm. If the thickness increases or decreases, the deviations will increase. It suggests that, to this motor at this power volume, yoke thickness at 10 mm is an optimal value.

This article has been accepted for publication in a future issue of this journal, but has not been fully edited. Content may change prior to final publication. Citation information: DOI 10.1109/TEC.2018.2815564, IEEE Transactions on Energy Conversion

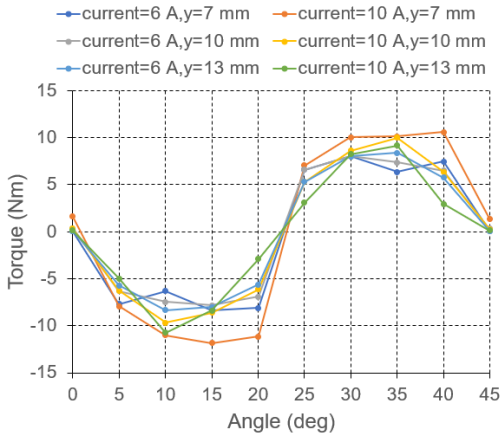

Fig.5 Torque outputs under different values of the thickness of move yoke.

V. Control Scheme and Experimental Validation

A. Control Scheme

The entire control block for the motor is shown Fig.6, including the linear and the rotary directions simultaneously. Two proportional-integral-derivation (PID) controllers are employed for the closed loop controls. The driver includes a current control loop by using pulse width modulation (PWM). The angle and position distribution block is used to calculating the forces and torques to each phases of the linear and rotary directions, respectively. Its detail is shown in Fig.7.

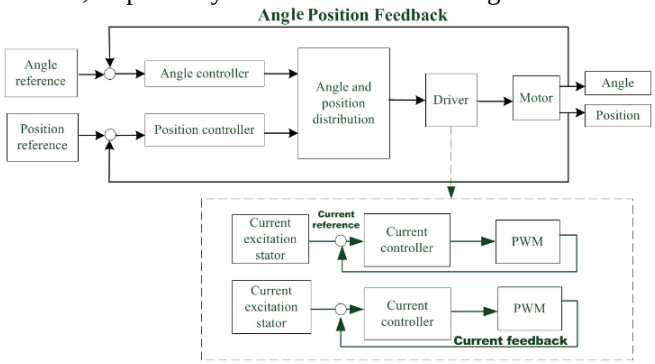

Fig.6. Control block for the proposed motor.

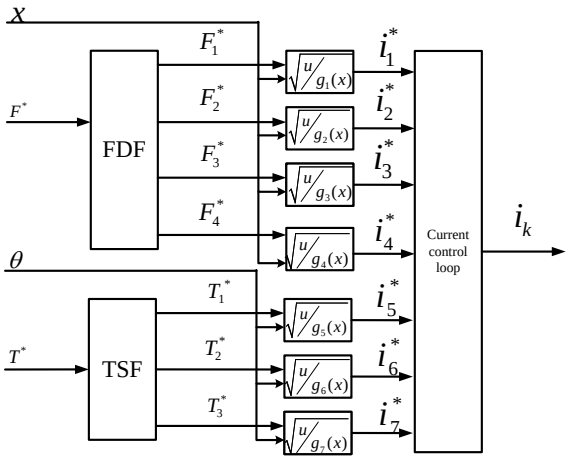

Fig.7 Angle and position distribution block

As adjacent phases of outside and inner stators have common conducting regions, a force distribution function (FDF) and a torque sharing function (TSF) are employed to alleviate ripples of the force and torque outputs [20], [21]. In Fig.7,

$$g_k(x) = \frac{1}{2} \cdot \frac{\partial L(i,x)}{\partial x}, \; k=1,2,3,4. \tag{14}$$

$$g_k(\theta) = \frac{1}{2} \cdot \frac{\partial L(i,\theta)}{\partial \theta}, \; k=5,6,7. \tag{15}$$

the current references can be calculated by using above equations. The conducting phases for FDF and TSF are listed in Table II and III.

TABLE II
CONDUCTING AREA FOR LINEAR MOTION

LINEAR (MM)	PHASE (+)	PHASE (-)
[0, 5.75)	B	AD
[5.75, 11.50)	BC	A
[11.50, 17.25)	C	BA
[17.25, 23.00)	CD	B
[23.00, 28.75)	D	CB
[28.75, 34.50)	DA	C
[34.50, 40.25)	A	DC
[40.25, 46.00)	AB	D

TABLE III
CONDUCTING REGION FOR ROTATION

LINEAR (mm)	PHASE (+)	PHASE (-)
[0, 7.50)	B	AC
[7.50, 15.00)	BC	A
[15.00, 22.50)	C	BA
[22.50, 30.00)	CA	B
[30.00, 37.25)	A	CB
[37.25, 45.00)	AB	C

As each direction of the motor can be controlled individually and the two dimensions are physically decoupled, their transfer blocks can be expressed by Fig.8 and their closed transfer functions can be formulated as equation (16). G_p is the block of the PID controller and N denotes the interference to the control system. The dynamic transfer function of the motor is a second order system with the parameters including M , B and A_1 are mainly determined by the mass of the mover, the fraction of the shaft.

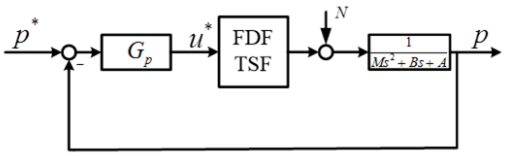

Fig.8 Control transfer function block of the motor

$$\frac{p}{p^*} = \frac{K_G K}{Ms^2 + Bs + (A_1 + K_G K)} \tag{16}$$

K_G is the proportion of the controller and K is the gain of the FDF or TSF blocks. The parameters of the two PID controllers are listed in Table III. The parameters for two controllers are listed in Table IV.

TABLE IV
PARAMETERS OF THE TWO PID CONTROLLERS

Controller	P	I	D
Position	5.1	0	0.08
Angle	4.8	0.024	0.18

This article has been accepted for publication in a future issue of this journal, but has not been fully edited. Content may change prior to final publication. Citation information: DOI 10.1109/TEC.2018.2815564, IEEE Transactions on Energy Conversion

B. Force Measurement

The force and torque outputs of the motor are measured by a force gauge and a torque meter, as shown in Fig.9 (a). A force gauge is fixed on the end of the motor by using a clamp. Another end of the force gauge is fixed on the ending section of the mover and the length of the force gauge can be regulated via a screw so that the linear position of the mover is adjustable. Therefore, the linear force outputs are obtained. Static values of force and torque corresponding to different positions and angles are given under a non-load condition in Fig.9 (b) and Fig.9 (c).

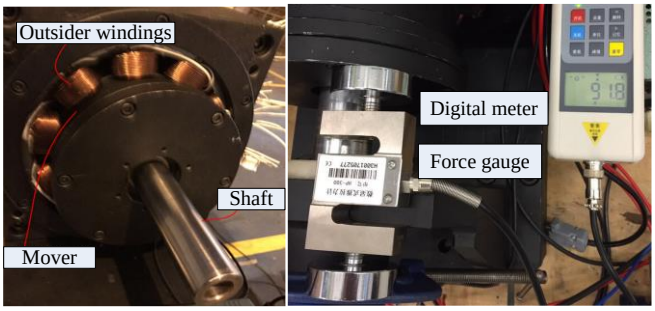

(a)

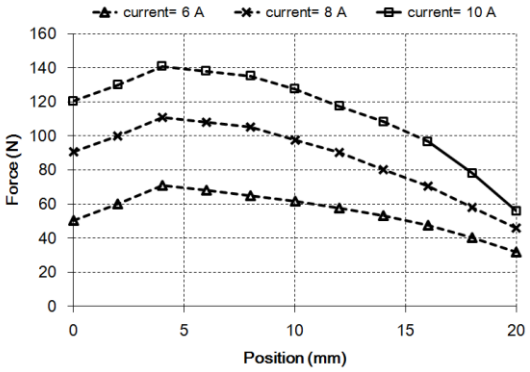

(b)

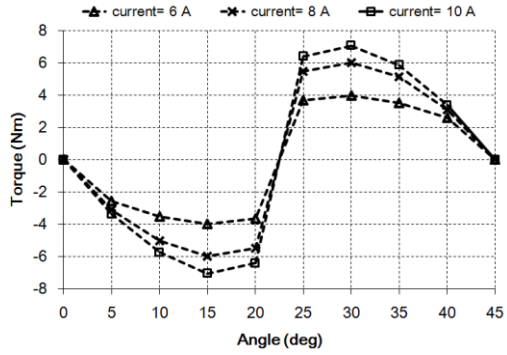

(c)

Fig.9 Measurements of the force and torque outputs

Form the measurement results, the force and torque features of the motor during a period fully agree with that by FEM. The maximum values of force output and torque output are 140 N and 6.5 Nm, respectively.

C. Control Experimental Results

The whole experimental set up consists of a computer, a dSPACE DS1104 card, a power supplier, a driver and the motor, as shown in Fig.10. The control scheme as well as the controllers is built using the software package MATLAB/Simulink. The entire Simulink software will be programmed and debugged into the dSPACE card which is regarded as a hardware controller. This control card outputs commands to the driver for the motor after getting the position and rotational feedbacks from two encoders fixed on the motor's shaft, constructing a closed loop control.

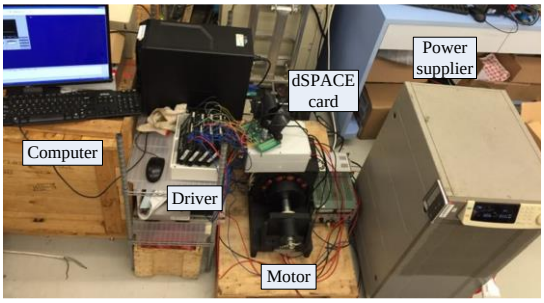

Fig.10 Photograph of the experimental setup of the control of the motor.

Sinusoidal references are given by the computer, as shown in Fig.11 (a), (b). The frequency of the references to linear motion and rotary motion is 1 Hz and the amplitudes of two references are 20 mm and 360 degree respectively. The corresponding references are 0.1 mm and 0.3 degree, as shown in Fig.11 (c) and (d).

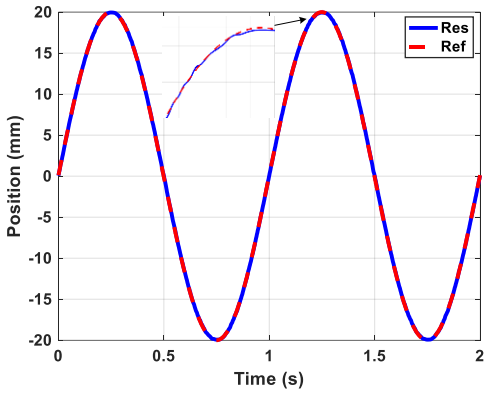

(a)

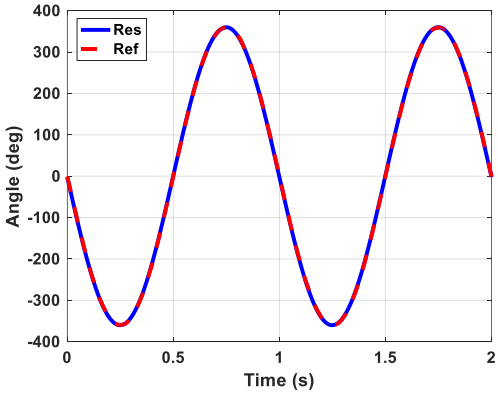

(b)

This article has been accepted for publication in a future issue of this journal, but has not been fully edited. Content may change prior to final publication. Citation information: DOI 10.1109/TEC.2018.2815564, IEEE Transactions on Energy Conversion

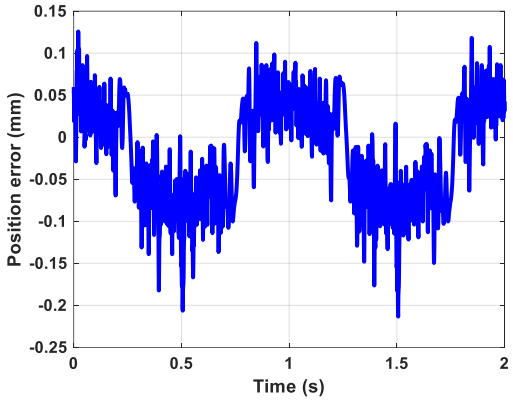

(c)

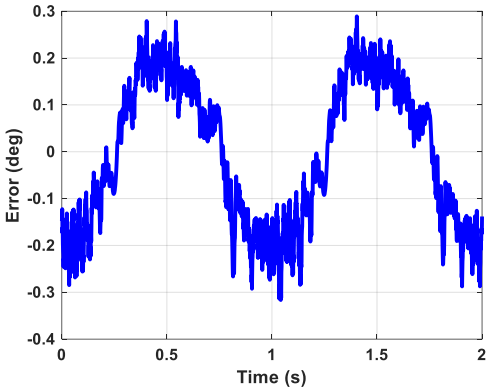

(d)

Fig.11.Response for linear motion (a) and (b) Rotary, and corresponding dynamic errors (c) and (d).

In order to investigate the performance of the motor with load, as shown in Fig. 12, loading test responses are given for the motor both in linear and rotary directions, under 90 N for linear movements and 3 N.m for rotation. Corresponding errors to the two responses with 0.5 Hz are obtained in Fig. 12 (b) and (d). The vibration frequencies of errors are alleviated because of the loads. The angle error and position error are regulated within 0.3 degree and 0.5 mm. This motor can also reach a precise tracking.

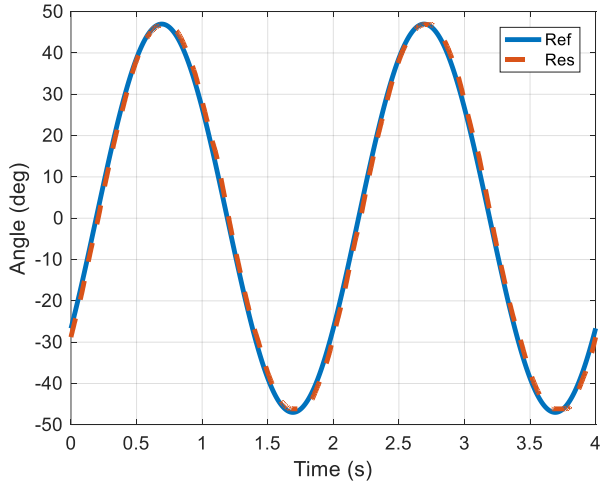

(a)

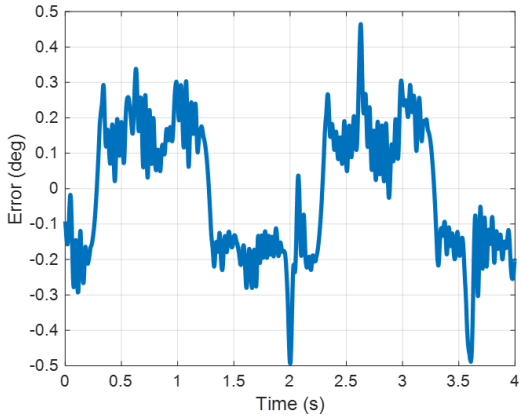

(b)

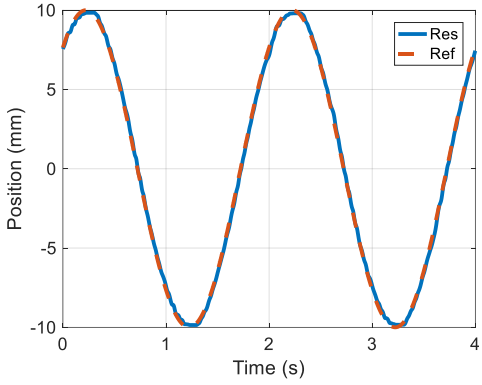

(c)

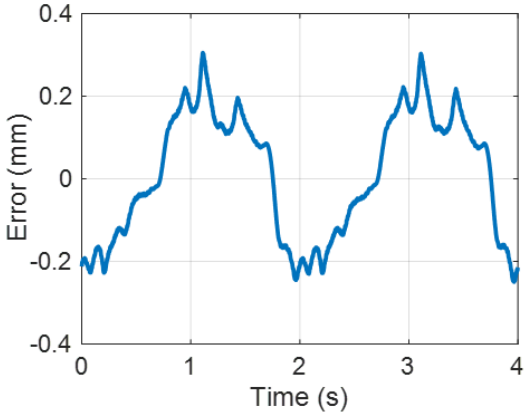

(d)

Fig.12. Dynamic response of linear motion (a) and errors for linear movements (c), and dynamic response of angles (c) and errors (d) with loads.

The simultaneous movements in linear and rotary directions are also obtained when the mover rotates at a constant speed of 500 rpm and the scope of the linear movement is under the scope of 20 mm under 0.5 Hz. In Fig. 13 (a), the linear movement response is plotted, and its error is given in Fig. 13 (b). From Fig. 13 (c), the speed is controlled at a constant speed with an error of 1 rpm. The phase currents of the motor are also measured as shown in Fig. 13 (d). There are some ripples of the currents. The currents need to be regulated in real time because of the varied torque outputs from the motor.

This article has been accepted for publication in a future issue of this journal, but has not been fully edited. Content may change prior to final publication. Citation information: DOI 10.1109/TEC.2018.2815564, IEEE Transactions on Energy Conversion

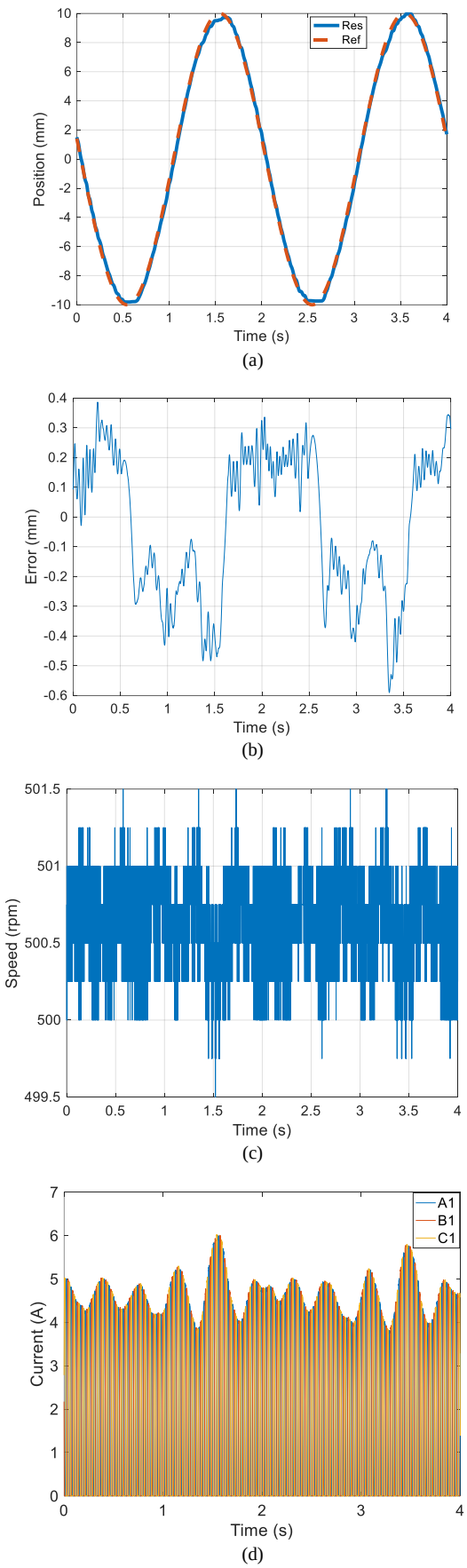

Fig.13. Dynamic response of linear motion (a) and errors for linear movements (c), and the speed tracking response (c) and phase currents (d).

VI. Conclusion

A novel RLSRM is designed and realized with a simple decoupled magnetic structure. Using a set of stacked steel plates realizes the decouple design magnetically, with short magnetic flux path employed both in the outside stator and the inner stator. Also, flux barriers are also added to modify the decoupled structure for the mover. The major design parameters are calculated, including both of the linear and rotary sections. The results of FEM study proved the feasibility of the RLSRM design. A simple control scheme is proposed for the motor to achieve a decoupled highly positioning tracking accuracy. Experimental results verify the effectiveness and feasibility of the designed motor, with tracking errors under loads less than 0.3° and 500 μm for the rotary and linear axes, respectively. The motor could achieve a linear force at 140 N, and a torque at 6.5 N·m at the same time, with the same current level.

References

[1] J. F. Pan, Yu Zou, N. C. Cheung, "Performance Analysis and Decoupling Control of an Integrated Rotary–Linear Machine with Coupled Magnetic Path," *IEEE Trans. Magn*., vol. 50, no. 2, Feb. 2014.

[2] R. Cao, M. Cheng, C. Mi, W. Hua, and W. Zhao, "Comparison of complementary and modular linear flux-switching motors with different mover and stator pole pitch," *IEEE Trans. Magn*., vol. 49, no. 4, pp. 1493–1504, Apr. 2013.

[3] C. T. Liu and T. S. Chiang, "Design and performance evaluation of a micro linear switched-reluctance motor," *IEEE Trans. Magn*., vol. 40, no. 2, pp. 806–809, Mar. 2004.

[4] G. Baoming, A. T. de Almeida, and F. Ferreira, "Design of transverse flux linear switched reluctance motor," *IEEE Trans. Magn*., vol. 45, pp. 113-119, 2009.

[5] K. J. Meessen, J. J. H. Paulides, and E. A. Lomonova, "Analysis of a novel magnetization pattern for 2-DoF rotary-linear actuators," *IEEE Trans. Magn*., vol. 48, no. 11, pp. 3867–3870, Nov. 2012.

[6] T. T. Overboom, J. W. Jansen, E. A. Lomonova, and F. J. F. Tacken, " Design and optimization of a rotary actuator for a two-degreeof freedom zϕ-module," *IEEE Trans. Ind. Appl*., vol. 46, no. 6, pp. 2401–2409, Nov./Dec. 2010.

[7] G. Krebs, A. Tounzi, B. Pauwels, D. Willemot, and F. Piriou, "Modeling of a linear and rotary permanent magnet actuator," *IEEE Trans. Magn*., vol. 44, no. 11, pp. 4357–4360, Nov. 2008.

[8] J. H. H. Alwash, A. D. Mohssen, and A. S. Abdi, "Helical motion tubular induction motor," *IEEE Trans. Energy Convers*., vol. 18, no. 3, pp. 362–369, Sep. 2003.

[9] Y. H. Kim, C. S. Jin, S. Kim, Y. D. Chun, and J. Lee, "Analysis of hybrid stepping motor using 3D equivalent magnetic circuit network method based on trapezoidal element," *J. Appl. Phys*., vol. 91, no. 10, pp. 8311–8313, 2002.

[10] X. D. Xue, K.W.E.Cheng, S.L. Ho, "A Self-Training Numerical Method to Calculate the Magnetic Characteristics for Switched Reluctance Motor Drives", *IEEE Trans. Magnetics*, vol. 40 , no. 2 , 2004, pp 734 – 737.

[11] Y. Sato, "Development of a 2-degree-of freedom rotational linear switched reluctance motor," *IEEE Trans. Magn*., vol. 43, no. 6, pp. 2564-2566, 2007.

[12] Mohammad Mehdi Nezamabadi, Ebrahim Afjei, and Hossein Torkaman, "Design, Dynamic Electromagnetic Analysis, FEM, and Fabrication of a New Switched-Reluctance Motor with Hybrid Motion," *IEEE Trans. Magn*., vol. 52, no. 4, April 2007.

[13] J.K.Lin, K.W.E.Cheng, "Active Suspension System Based on Linear Switched Reluctance Actuator and Control Schemes", *IEEE Transactions on Vehicular Technology*, vol. 62, Issue: 2, 2013, pp. 562 – 572.

[14] Liu C T and Kuo J L, "Experimental investigation and 3-D modeling of linear variable reluctance machine with magnetic-flux decoupled windings," *IEEE Trans. Magn*., vol. 30, pp. 4737–4739, Nov. 1994.

[15] J. F. Pan, Yu Zou, Guangzhong Cao, "An Asymmetric Linear Switched Reluctance Motor," *IEEE Trans. Energy Convers.*, vol. 28, 2, pp. 444–451, 2013.

[16] J. F. Pan, Norbert C. Cheung, Yu Zou, "Design and Analysis of a Novel Transverse-Flux Tubular Linear Machine with Gear-Shaped Teeth Structure," *IEEE Trans. Magn*., vol. 48, pp. 3339–3343, Nov. 2012.
[17] J. F. Pan, Norbert C. Cheung, Yu Zou, "An Improved Force Distribution Function for Linear Switched Reluctance Motor on Force Ripple Minimization with Nonlinear Inductance Modeling," *IEEE Trans. Magn*., vol. 48(11), pp. 3064 – 3067, 2012.
[18] T. J. Miller. Electronic control of switched reluctance machines, *Newnes Power Engineering Series*, US, pp.68-72, 2001.
[19] T. J. E. Miller, Switched Reluctance Motors and Their Controls. *Magna Physics Publ*., 1993.
[20] J.W. Zhu, K.W.E. Cheng, X.D. Xue, Yu Zou, "Design of a New Enhanced Torque In-Wheel Switched Reluctance Motor with Divided Teeth for Electric Vehicles", *IEEE Trans. Magnetics, 2017*, Vol. 53, Issue 11.
[21] X. D. Xue, K. W. E. Cheng, S. L. Ho, "Optimization and Evaluation of Torque-Sharing Functions for Torque Ripple Minimization in Switched Reluctance Motor Drives," *IEEE Trans. power electronics.*, 24(9), pp.2076-2090, 2009.

Li Siyang obtained his BSc degrees from the South China University of Technology in 2012. He is currently pursuing his Ph.D degree under the supervision of Professor Cheng at the Power Electronics Research Centre in the Hong Kong Polytechnic University.
Her research interest mainly focuses on the, Energy conversion, Solar tracking system for CPV power generation system, Design and control the SR motor, as well as energy storage,

K.W.E.Cheng obtained his BSc and PhD degrees both from the University of Bath in 1987 and 1990 respectively. Before he joined the Hong Kong Polytechnic University in 1997, he was with Lucas Aerospace, United Kingdom as a Principal Engineer.
Dr. Cheng was the recipient of the Institution of Electrical Engineers Sebastian Z De Ferranti Premium Award in 1995, the Outstanding Consultancy Award in 2000, the Faculty Merit Award for Best Teaching in 2003 from Hong Kong Polytechnic University, the Faculty Engineering Industrial and Engineering Services Grant Achievement Award in 2006, the Brussels Innova Energy Gold Medal with Mention in 2007, the Consumer Product Design Award in 2008, the Electric Vehicle Team Merit Award of the Faculty in 2009, the Geneva Invention Expo Silver Medal in 2011, the Eco Star Award in 2012, Gold prize at Seoul International Invention Fair in 2005 and iCAN Gold medal at Canada in 2016. He is now the professor and director of Power Electronics Research Centre.

N. C. Cheung received the B.Sc. degree from the University of London, London, U.K., the M.Sc. degree from the University of Hong Kong, Hong Kong, and the Ph.D. degree from the University of New South Wales, Sydney, Australia, in 1981, 1987, and 1995, respectively. He is currently with the Department of Electrical Engineering, Hong Kong Polytechnic University, Hong Kong. His research interests are motion control, actuator design, and power electronic drive.

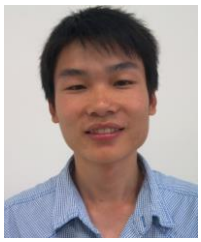

Yu Zou obtained his B.S. degree from Hubei University in 2010 and Master degree at College of Mechatronics and Control Engineering at Shenzhen University in 2013. He is now pursuing his Ph.D degree at The Hong Kong Polytechnic University.